Metastability in Chemotaxis Models[*]

A. B. Potapov[1] and T. Hillen[1,2]

We consider pattern formation in a chemotaxis model with a vanishing chemotaxis coefficient at high population densities. This model was developed in Hillen and Painter (2001, *Adv. Appli. Math.* **26**(4), 280–301.) to model volume effects. The solutions show spatio-temporal patterns which allow for ultra-long transients and merging or coarsening. We study the underlying bifurcation structure and show that the existence time for the pseudo-structures exponentially grows with the size of the system. We give approximations for one-step steady state solutions. We show that patterns with two or more steps are metastable and we approximate the two-step interaction using asymptotic expansions. This covers the basic effects of coarsening/merging and dissolving of local maxima. These effects are similar to pattern dynamics in other chemotaxis models, in spinodal decomposition of Cahn–Hilliard models, or to metastable patterns in microwave heating models.

1. INTRODUCTION

Chemotaxis is an important mechanism that controls the movement of many organisms. For example, slime molds are able to detect a chemical gradient and move toward high concentrations of a chemoattractant. The most prominent model for this process is the Patlak–Keller–Segel model (PKS) [10,11,13]

---

[1] Centre for Mathematical Biology, University of Alberta, Edmonton, Alberta, Canada, T6G 2G1. E-mail: {apotapov,thillen}@math.ualberta.ca
[2] To whom correspondence should be addressed.

293

$$u_t = \text{div}(D_1(u, S)\nabla u - \chi(u, S)u\nabla S),$$
$$\tau S_t = D_2\Delta S + k(u, S),$$
$$u = u(x, t), \quad S = S(x, t), \quad x \in \Omega \subset R^n,$$
$$\partial_n u|_\Omega = \partial_n S|_\Omega = 0,$$

(1)

where $u(x, t)$ denotes the particle distribution function and $S(x, t)$ is the concentration of a chemical signal. The *motility* $D_1(u, S)$ and the *chemotactic sensitivity* $\chi(u, S)$ depend on the particle density and on the signal concentration. The term $k(u, S)$ describes production and decay or consumption of the signal and D_2 is the diffusion constant for S. The parameter τ indicates that movement of the species and dynamics of the signal have different characteristic time scales.

The qualitative properties of the PKS model (1) strongly depend on the actual form of the coefficients, and on the dimension of the problem. For example for $D_1 = $ constant, $\chi = $ constant and $k = \alpha u - \beta S$ it is known that solutions of (1) in two or three dimensions can blow-up in finite time. For details see the reviews of Horstmann [7,8].

Hillen and Painter [6,12] included volume effects. As soon as a maximal cell density is reached, no more cells can be added to that location. The modeling of this *volume filling* effect leads, in a special case, to the following parameters:

$$D_1(u, S) = \text{const.},$$
$$\chi(u, S) = \chi \cdot (1 - u),$$
$$k(u, S) = \alpha u - \beta S.$$

(2)

So the equations take the form:

$$u_t = D_1 u_{xx} - \chi (u(1 - u)S_x)_x,$$
$$\tau S_t = D_2 S_{xx} + \alpha u - \beta S,$$
$$0 < x < L,$$

(3)

$$u_x|_{x=0,L} = S_x|_{x=0,L} = 0,$$
$$u(x, 0) = u_I(x), \quad S(x, 0) = S_I(x).$$

(4)

This model has been studied in [6]. There global existence of the solution has been proven and an interesting effect has been observed in numerical calculations. Let us take the initial data as a perturbation of the spatially homogeneous background. After a rather short transition period a structure with a number of "steps" arises. It stays almost unchanged for a rather long period, then comparatively quickly some steps "annihilate", and a transition to a smaller number of steps occurs. The new structure
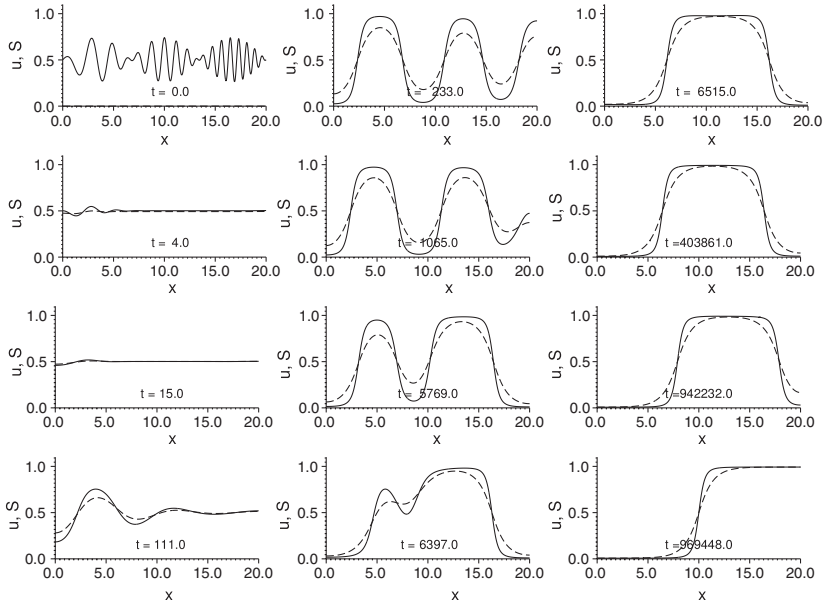
Figure 1. Example of pseudostructures in model (3), $\tau = D_2 = \alpha = \chi = \beta = 1$, $D_1 = 0.1$, $L = 20$, $M = 0.5$, the value of t is shown at every panel. The solid line is u, the dashed line is S. We observe a transition of a five-step pattern at $t = 233.0$ to a one-step pattern at $t = 10^6$. Note that the two-step pattern exists from $t = 6.5 \times 10^3$ to $t = 10^6$, i.e. during about 10^6 time units.

can stand unchanged even longer, then a new merger occurs and so on. The most unusual thing is the duration of such transitions—up to 10^8 time units and more, depending on the parameters of the model. Figure 1 shows an example of the described process. First we observe a transitional period where some frequencies are damped and others are enhanced until at $t = 233.0$ a five-step pattern appears. The right step vanishes at about $t = 1065.0$ and a four-step pattern develops. This four-step pattern becomes a two-step solution at about $t = 6515.0$ and finally a one-step solution appears ($t = 10^6$). Varying system parameters it is possible to increase this time, e.g. in [6] authors observed a transient period of duration about 10^9. In practice such metastable patterns may be indistinguishable from true stable solutions.

Figure 2 shows the rate of change of u and S over time. The transformations of the structure are clearly visible as the peaks of u_t and S_t. We call such formations 'pseudostructures' or 'metastable solutions'. In spite of their transitional nature they may strongly influence the dynamics of the processes if the transition time is comparable to the lifetime of the system.
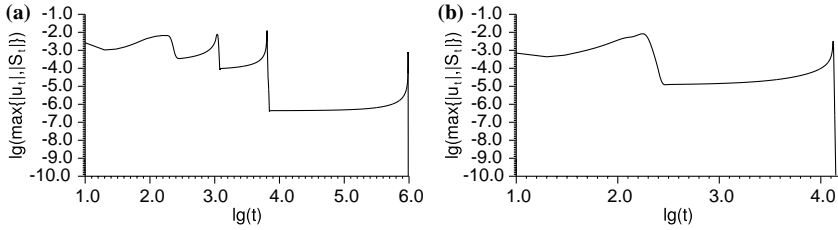
Figure 2. (a) Rate of change for u and S from Fig. 1 over time in a doubly-logarithmic plot, $\lg\left(\max\{|u_t|, |S_t|\}\right)$. The long plateaus between $\lg t \approx 2.5$, 4, and 6 correspond to pseudo-structures with 5, 4 and 2 steps, respectively (note the logarithmic scale in t). The peaks correspond to merging or coarsening events. (b) Same as above on a shorter interval, $L = 10$. Decrease of L from 20 to 10 considerably shortens the transition times and the duration of pseudostructure existence.

We present a detailed study of this effect in the chemotaxis model, and show that it can arise in other models as well. From the dynamical systems point of view pseudostructures correspond to saddle points with very weak instability. On short time scales such saddles may be almost indistinguishable from true attractors.

We also note that very long transients have been observed in other models before, e.g. in Cahn–Hilliard equations [1, 16], in coupled map lattices [2], in microwave heating [9], or in other chemotaxis models.

The paper is organized as follows. In Section 1.1 we reduce the number of relevant model parameters and we formulate the problem under investigation (5)–(7). In Section 2 we present a result on linear stability of the homogeneous steady state. In Section 3 we consider an elliptic problem which characterizes the non-homogeneous steady states and we study the underlying bifurcations. It turns out that all stationary solutions with more than one transition layer ("step") are saddle points with ultra small unstable eigenvalues ("metastability"). In Section 4 we give a constructive approximation of the transition layers. Moreover, we analyze the interaction of transition layers using perturbation methods. A possible explanation of coarsening and merging is given. In addition, we consider the approach to metastability which was used by Ward [9] for the microwave heating equations. The method seems formally applicable, although additional work is required to justify the approximations. In Section 5 we present alternative models which produce very similar pseudo-structures.

1.1. Reducing the Number of Parameters

Equation (3) includes seven-parameters. For convenience we reduce this set to four essential parameters. First we rescale D_2, α and β to make

$\tau = 1$. Second, we are interested in the case when $\chi \neq 0$, otherwise the dynamics become trivial. Also we shall assume $D_1 \neq 0$. Then it is convenient to make the following change:

$$\hat{S} = \frac{\chi S}{D_1}, \quad \eta = \frac{\alpha \chi}{D_1}.$$

Omitting the hat, we come to the following system which is the focus of our studies in this paper:

$$u_t = D_1 (u_x - u(1-u)S_x)_x, \tag{5}$$
$$S_t = D_2 S_{xx} + \eta u - \beta S, \tag{6}$$
$$u_x|_{x=0,L} = S_x|_{x=0,L} = 0, \tag{7}$$
$$u(x,0) = u_0(x), \quad S(x,0) = S_0(x).$$

It is also possible to set two of the three parameters D_1, D_2, and L equal to 1, but we shall not do so to make the comparison with previous results easier.

Note that this system has one conserved quantity,

$$M = \frac{1}{L} \int_0^L u(x,t)\mathrm{d}x = \frac{1}{L} \int_0^L u(x,0)\mathrm{d}x.$$

Therefore, the problem has an implicit parameter, M. According to the results of Hillen and Painter [6], Eq. (3) have an invariant region $\Gamma = \{0 \leqslant u \leqslant 1, 0 \leqslant S \leqslant \eta/\beta\}$. We consider only values of M with $0 \leqslant M \leqslant 1$.

System (5), (6) is symmetric with respect to $u = 0.5$.

Lemma 1.1. *If (u, S) is a solution of system (5), (6) with $(u(x,t), S(x,t)) \in \Gamma$, for $M = M_1$, $0 \leqslant M_1 \leqslant 1$, then $(1-u, \eta/\beta - S)$ is a solution of the same system for $M_2 = 1 - M_1$.*

Proof. This is a straightforward calculation. $\qquad \square$

Below we shall study both stationary and nonstationary solutions. To distinguish between them we shall explicitly show their arguments where necessary, e.g., $u(x,t)$ for a nonstationary solution and $u(x)$ for a stationary one.

2. SPATIALLY HOMOGENEOUS SOLUTIONS AND THEIR STABILITY

Equations (5) and (6) have the spatially homogeneous solution $u = M$, $S = \eta M/\beta$. It is a natural first step to study its stability.

Theorem 2.1. Let D_1, D_2, η, β, M be positive, and assume there exists $k \in \mathbb{N}$ such that the inequalities

$$0 < \left(\frac{\pi k}{L}\right)^2 < \mu_* \tag{8}$$

hold, where

$$\mu_* = \frac{\eta M (1 - M) - \beta}{D_2}. \tag{9}$$

Then

1. The spatially homogeneous solution of (5), (6), (7) is linearly unstable.
2. The number of unstable Fourier modes k_u equals the greatest k satisfying (8), that is $k_u \approx L\sqrt{\mu_*}/\pi$;
3. the most unstable mode is of the form $k = \left[L\sqrt{\mu_U}/\pi\right]$ or $k = \left[L\sqrt{\mu_U}/\pi\right] + 1$, where $[\cdot]$ denotes the integer part and μ_U satisfies

$$\mu_U > \frac{\sqrt{D_1 D_2}}{\left(\sqrt{D_1} + \sqrt{D_2}\right)^2} \mu_*. \tag{10}$$

That is the wavenumber of the most unstable mode k increases with μ_* and hence with η.

Proof. Let us set $u = M + \tilde{u}$, $S = \eta M/\beta + \tilde{S}$, and linearize the equations. This gives

$$\tilde{u}_t = D_1(\tilde{u}_{xx} - M(1 - M)\tilde{S}_{xx}), \tag{11}$$

$$\tilde{S}_t = D_2\tilde{S}_{xx} + \eta\tilde{u} - \beta\tilde{S}, \tag{12}$$

$$\tilde{u}_x = \tilde{S}_x = 0, \quad x = 0, L. \tag{13}$$

The kth Fourier mode $\cos((\pi k x)/L)$, $k \in \mathbb{N}$, grows as $\exp(\nu t)$, where ν is the largest eigenvalue of the matrix

$$A(\mu) = \begin{pmatrix} -D_1\mu & M(1 - M)D_1\mu \\ \eta & -D_2\mu - \beta \end{pmatrix}, \quad \mu = \left(\frac{\pi k}{L}\right)^2.$$

In spite of the fact that μ takes only discrete values, it is convenient to consider it as a continuous variable. For the eigenvalue ν we have the equation

$$\nu^2 - \mathrm{tr}A\,\nu + \det A = 0, \tag{14}$$

where $\mathrm{tr}\, A = -(D_1 + D_2)\,\mu - \beta < 0$ and

$$\det A = D_1\mu\,(D_2\mu + \beta - \eta M(1 - M)) = -D_1 D_2 \mu\,(\mu_* - \mu).$$

The discriminant of (14) is

$$
\begin{aligned}
d &= (\mathrm{tr}\, A)^2 - 4\det A = (D_1 - D_2)^2\,\mu^2 + \beta^2 + 2\beta\,(D_1 + D_2)\,\mu + 4D_1 D_2\mu_*\mu \\
&\geqslant (D_1 - D_2)^2\,\mu^2 + \beta^2 - 2\beta\,(D_1 - D_2)\,\mu \geqslant 0,
\end{aligned}
$$

since $\mu_* > -\beta/D_2$. Hence the roots of (14) are always real, and the largest root

$$\nu = (\mathrm{tr}\, A + \sqrt{d})/2 \tag{15}$$

is positive only if $\det A < 0$, that is $0 < \mu < \mu_*$. This means that on a bounded domain $[0, L]$ with Neumann boundary conditions we find a finite set of unstable modes $k \in \mathbb{N}$

$$0 < k < \frac{L}{\pi}\sqrt{\mu_*}. \tag{16}$$

This proves statements 1 and 2.

To prove statement 3 let us consider ν as a continuous function of μ. A typical dependence $\nu(\mu)$ is plotted in Fig. 3. Let us denote the position of the maximum of $\nu(\mu)$ by μ_U. To find the value of μ_U we have to solve the equation $\mathrm{d}\nu/\mathrm{d}\mu = 0$. Direct differentiation of (15) gives intractable results, so we introduce a new function $\phi(\mu) = 2\nu - \mathrm{tr}\, A$. Since $\mathrm{tr}\, A$ is a linear function of μ, the condition $\mathrm{d}\nu/\mathrm{d}\mu = 0$ is equivalent to $\mathrm{d}\phi/\mathrm{d}\mu = -\mathrm{d}\mathrm{tr}\, A/\mathrm{d}\mu = D_1 + D_2$. From (15) it follows that $\phi^2 = (\mathrm{tr}\, A)^2 - 4\det A$. Differentiating this expression by μ we obtain

$$2\phi\phi_\mu = 2\mathrm{tr}\, A\,(\mathrm{tr}\, A)_\mu - 4\,(\det A)_\mu.$$

Then taking the square of both sides and substituting the expressions for ϕ^2 and $\mathrm{d}\phi/\mathrm{d}\mu$ we come to

$$
\begin{aligned}
&4(((D_1 + D_2)\,\mu + \beta)^2 + 4D_1 D_2\mu\,(\mu_* - \mu))\,(D_1 + D_2)^2 \\
&= [2\,((D_1 + D_2)\,\mu + \beta)\,(D_1 + D_2) + 4D_1 D_2\,(\mu_* - 2\mu)]^2.
\end{aligned}
$$

It is convenient to introduce

$$a = \frac{D_1 + D_2}{D_1 D_2}, \qquad D_1 + D_2 = a D_1 D_2.$$

Then after simplification we obtain

$$(D_1 D_2 a^2 - 4)\mu^2 + 2\,(2\mu_* + a\beta)\,\mu - \mu_*\,(\mu_* + a\beta) = 0$$

and the only positive root is

$$\mu_U = \frac{\mu_* \, (\mu_* + a\beta)}{2\mu_* + a\beta + a\sqrt{\beta^2 + D_1 D_2 \mu_* \, (\mu_* + a\beta)}}.$$

The numerator is a quadratic function of μ_*, while the denominator for large μ_* behaves like a linear function. Therefore, as μ_* increases, the wavenumber of the most unstable mode increases too. Let us find a lower bound for the growth rate of $\mu_U(\mu_*)$.

Differentiating the quotient μ_U/μ_* by μ_* one can see that the derivative is negative, therefore μ_U/μ_* is a monotonically decreasing function of μ_* (we omit the details because they are straightforward but lead to quite long formulas). Therefore

$$\frac{\mu_U}{\mu_*} > \lim_{\mu_* \to \infty} \left(\frac{\mu_U}{\mu_*} \right) = \frac{1}{2 + a\sqrt{D_1 D_2}} = \frac{\sqrt{D_1 D_2}}{\left(\sqrt{D_1} + \sqrt{D_2} \right)^2}.$$

Hence we come to (10).   □

It follows from the theorem that for a large interval length L we should expect that initial instability will develop into a structure having more than one step. For the parameters in Fig. 1 we have $\mu_* = 1.5$, $\mu_U = 0.57$, there are seven unstable Fourier modes, and the most unstable is the 5th one. Therefore linear analysis explains why the structure developed from the perturbed homogeneous background with five steps.

Note 1. We see from (9) that for $M \to 0$ or $M \to 1$ the value of μ_* goes to 0 or may even become negative. Hence spatially uniform solutions with M close enough to 0 or 1 are always stable. Below we shall see that this feature is important for the formation of step-like structures:
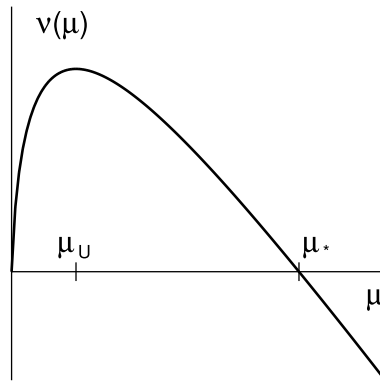

Figure 3. Sketch of the dependence of the unstable eigenvalues $\nu(\mu)$ on μ.

when the spatially homogeneous solution becomes unstable, chemotaxis "pumps" the particles to sub-domains with the stable level of u close to 1 and outside of them there is also a stable level close to 0. The sizes of these sub-domains are balanced to keep the average value the same.

Note 2. From linear analysis and numerics we can see, that typically a first appearance of steps is comparatively fast. The first pattern splits the interval $[0, L]$ into subintervals of characteristic length close to $\pi/\sqrt{\mu_U}$. Each of these subintervals contains one step. In these steps chemotactic forces are balanced by diffusion, and the subsequent evolution slows down.

Now let us consider two other problems: why the multi-step structure decays and why the transitions are extremely slow. To answer the questions we need to study stationary solutions and their stability.

3. STATIONARY SOLUTIONS

3.1. Equation for Stationary Solutions

Setting $u_t = 0$ in (5) we obtain

$$u_x - u(1-u)S_x = C = \text{const.}$$

Due to the boundary conditions (4), $C = 0$. Assuming that $0 < u < 1$ [6], we have

$$\frac{u_x}{u(1-u)} = S_x, \qquad \ln\frac{u}{1-u} = S - S_0, \qquad u = \frac{1}{1+e^{S_0-S}} \equiv \varphi(S, S_0). \quad (17)$$

The integration constant S_0 is determined from the conservation law

$$\frac{1}{L}\int_0^L \frac{\mathrm{d}x}{1+e^{S_0-S}} = M. \quad (18)$$

Note that Eq. (18) is a condition on S_0. Hence S_0 depends nonlocally on S, which we denote by $S_0[S]$. Substituting (17) into (6) we come to an elliptic problem

$$D_2 S_{xx} + \frac{\eta}{1+e^{S_0[S]-S}} - \beta S = 0, \quad S_x(0) = S_x(L) = 0. \quad (19)$$

Integrating this equation from 0 to L and taking into account boundary conditions and the conservation law (18), we obtain an additional integral relation for stationary profiles of $S(x)$

$$\eta M = \beta \frac{1}{L}\int_0^L S\mathrm{d}x. \quad (20)$$

For the spatially uniform solution $u = M$, $S = \eta M/\beta$, S_0 can be obtained explicitly

$$\frac{1}{1 + e^{S_0 - \eta M/\beta}} = M, \qquad S_0 = \frac{\eta M}{\beta} + \ln\left(\frac{1-M}{M}\right). \tag{21}$$

In other cases $S_0[S]$ is obtained numerically.

3.2. Spatially Inhomogeneous Solutions: Phase Plane Analysis

To analyze the properties of spatially inhomogeneous solutions it is convenient to denote $S_x = w$, moreover, we treat $S_0[S]$ to be a given constant. Then Eq. (19) is equivalent to the dynamical system

$$S_x = w, \tag{22}$$

$$D_2 w_x = \beta\,(S - f(S)), \qquad f(S) = \frac{\eta}{\beta}\frac{1}{1 + e^{S_0 - S}}, \tag{23}$$

with x playing the role of time. For constant S_0 this is a Hamiltonian system with the Hamiltonian

$$H(w, S) = \frac{1}{2}w^2 + \frac{\eta}{D_2}\ln(1 + e^{S - S_0}) - \frac{\beta}{2D_2}S^2,$$

therefore it can have fixed points of only two types, saddles and centers.

The properties of the system depend on the values of η/β and S_0. Its fixed points are located at $\bar{w} = 0$ and $\bar{S} = f(\bar{S})$. The function $f(S)$ is a sigmoid curve with $f(0) = \eta/\beta(1 + e^{S_0})^{-1} > 0$ and asymptote $f(+\infty) = \eta/\beta$. Typically the equation $\bar{S} = f(\bar{S})$ has one or three roots $\bar{S}_k$, see Fig. 4. Usually $\bar{S}_k$ can be found only numerically, but for the special case of $S_0 = \eta/2\beta$ one of the roots is $\bar{S} = S_0$. Comparing this value with (21) one can see that it can occur in the original system only if $M = 1/2$.

The eigenvalues $v_{1,2}$ for the fixed point $(\bar{S}_k, 0)$ are determined by

$$D_2 v^2 = \beta(1 - f'(\bar{S}_k)). \tag{24}$$

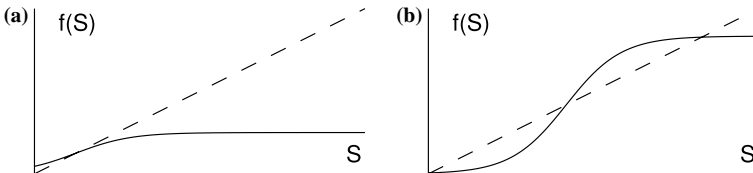Therefore for $f'(\bar{S}_k) < 1$ we have a saddle, while for $f'(\bar{S}_k) > 1$—a center.

Figure 4. The equation $f(S) = S$ typically has one root (a), or three roots (b).

In case of one root we have always $f'(\bar{S}_k) < 1$, a saddle (Fig. 4a), this occurs either when $\max_S f'(S) = f'(S_0) < 1$, that is $\eta < 4\beta$, or when S_0 deviates too strongly from $\eta/2\beta$. In case of three roots $\bar{S}_1 < \bar{S}_2 < \bar{S}_3$ (Fig. 4b) we have saddles at $\bar{S}_1$ and $\bar{S}_3$, and one center at $\bar{S}_2$. The corresponding phase plane portraits are shown in Fig. 5.

Now let us return to the solutions of the boundary value problem (19). Fixed points correspond to a spatially homogeneous solution, if there are more than one fixed point then only one of them satisfies (18) and hence represents a solution of (19). For this solution we have $\bar{S}_k = \eta M/\beta$, and S_0 is given by (21).

To get a spatially inhomogeneous solution we need a part of the trajectory of (22), (23) that (i) begins and ends at the line $w = 0$ to satisfy the boundary conditions and (ii) has transition "duration" between the two points equal to L. It is easy to see that only some of the periodic trajectories circling around the center can satisfy these two conditions (Fig. 5).

We parameterize the possible candidates for nonhomogeneous steady states by the point $(0, \hat{S})$ with $\bar{S}_2 \leqslant \hat{S} \leqslant \bar{S}_3$, where the trajectory hits the S-axis. Let $\hat{L}(\hat{S})$ denote the length of a half circle which ends at $(0, \hat{S})$. As $\hat{S}$ approaches $\bar{S}_3$ the corresponding orbit approaches a homoclinic, or a heteroclinic orbit (see Fig. 5), hence

$$\lim_{\hat{S} \to \bar{S}_3} \hat{L}(\hat{S}) = +\infty.$$

If $\hat{S}$ approaches $\bar{S}_2$, then the linearization around the center $\bar{S}_2$ gives the length of the corresponding half circle

$$\lim_{\hat{S} \to \bar{S}_2} \hat{L}(\hat{S}) = L^* := \frac{\pi}{\sqrt{\frac{\beta}{D_2}(f'(\bar{S}_2) - 1)}}.$$

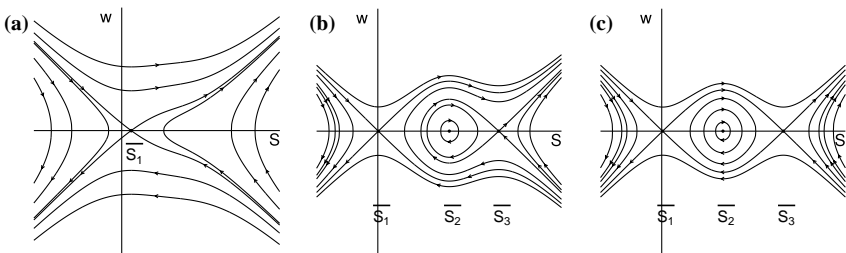In general, for interval length $L > L^*$ we have at least one, but maybe more, inhomogeneous steady states.

Figure 5. Typical phase plane portraits for the Hamiltonian system (22), (23). (a) one root of $S = f(S)$; (b) three roots, general S_0 choice; (c) three roots, special choice of $S_0 = \eta/2\beta$.

3.3. Bifurcations from the Spatially Uniform Solution

Bifurcations off the stationary spatially uniform solution of the Keller–Segel model have been analyzed in [14]. However, the results do not apply here due to the additional volume filling term.

From the above phase plane analysis it immediately follows that bifurcation points correspond to the cases when a new unstable mode is born, that is when $(L/\pi)\sqrt{\mu_*}$ takes integer values. If we use η as a bifurcation parameter, then the bifurcation points are

$$\eta_k = \frac{D_2\left(\frac{\pi k}{L}\right)^2 + \beta}{M(1 - M)},$$

see also [14].

According to linear stability analysis in the previous section, all bifurcating solutions with $k > 1$ are born unstable since all perturbations $a_n \cos((\pi n x)/L)$, $n < k$, have $\nu_n > 0$. Therefore, stable solutions can appear only after the first bifurcation, at $\eta = \eta_1$. In this case stability of the appearing solution depends on the type of the bifurcation: for supercritical bifurcation it is stable, for subcritical—unstable (see corresponding results in [14]).

To analyze the bifurcation type we use expansion of the following type:

$$\eta = \eta_1 + \gamma_1 \epsilon + \gamma_2 \epsilon^2 + \gamma_3 \epsilon^3 + \gamma_4 \epsilon^4 + \gamma_5 \epsilon^5,$$

$$S - S_0 = \sigma = -\ln\left(\frac{1 - M}{M}\right) + \sigma_1 \epsilon + \sigma_2 \epsilon^2 + \sigma_3 \epsilon^3 + \sigma_4 \epsilon^4 + \sigma_5 \epsilon^5,$$

$$S_0 = \frac{\eta_1 M}{\beta} + \ln\left(\frac{1 - M}{M}\right) + S_{01} \epsilon + S_{02} \epsilon^2 + S_{03} \epsilon^3 + S_{04} \epsilon^4 + S_{05} \epsilon^5$$

with

$$\sigma_n = \sum_{k=1}^{n} A_{nk} \cos\left(\frac{\pi k x}{L}\right).$$

Substituting these expressions into (19) we obtain $\gamma_1 = 0$, and hence the type of bifurcation depends on the sign of γ_2,

$$\gamma_2 = \frac{\eta_1 A_{11}^2}{6\mu D_2}\left((22\mu_1 D_2 + 4\beta)M(1 - M) - (4\mu_1 D_2 + \beta)\right).$$

The parameter γ_2 becomes zero if

$$M(1-M) = \frac{4\mu_1 D_2 + \beta}{22\mu_1 D_2 + 4\beta}$$

or

$$M_{c1,2} = \frac{1}{2} \pm \frac{1}{2}\sqrt{\frac{3\mu_1 D_2}{11\mu_1 D_2 + 2\beta}}.$$

Therefore for $M_{c1} > M > M_{c2}$ we have supercritical bifurcation, while for $M > M_{c1}$ or $M < M_{c2}$—subcritical bifurcation. Numerical experiments confirm that the solutions after the supercritical bifurcation are stable, whereas they are unstable after a subcritical bifurcation. In the latter case on the bifurcation branch there is a turning point, after which stable non-uniform solutions appear. We observed this turning point numerically.

Figures 6 and 7 show the numerical examples of bifurcations: the dependence of maximal and minimal values of spatially nonuniform solutions $S(x)$ on η (Fig. 6), and the corresponding S_0 (Fig. 7). Note that S_0 depends on the steady state by (18). We show the dependence of S_0 on η in Fig. 7 since we need a good approximation for S_0 later.

Summing up we may note the following. There are stationary solutions with a different number of "steps", arising from Fourier modes
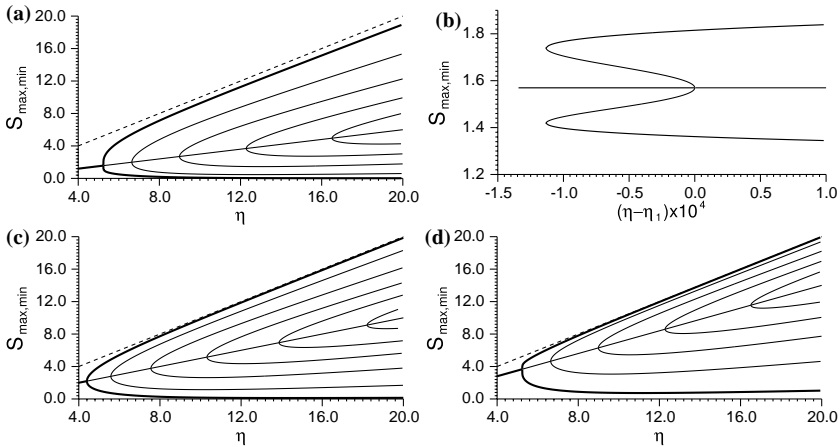

Figure 6. Bifurcation diagram of $S_{\max,\min}$ as a function of η. The mean density is $M = 0.3$ in (a,b), 0.5 in (c) and 0.7 (d). Other parameters: $D_2 = \beta = 1$, $L = 10$. (b) is an enlargement of the first bifurcation point from (a). Thick lines correspond to stable branches, thin to unstable branches. The dashed lines shows $S = \eta/\beta$. Solid straight lines corresponds to the spatially homogeneous solution, which loses its stability at the first bifurcation point, where the 1-step solution arises. This bifurcation can be both supercritical (c) and subcritical (a,d).
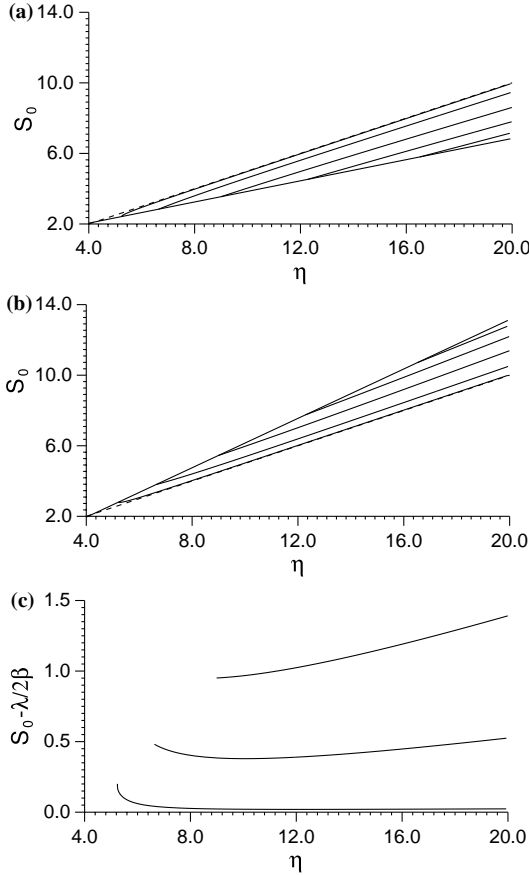
Figure 7.   The values of S_0 corresponding to the bifurcation diagrams in Figure 6 with $M = 0.3$ (a) and $M = 0.7$ (b). In the case of $M = 0.5$ we have $S_0 = \eta/2\beta$. The different lines in (a) and (b) correspond to the different bifurcation branches as seen in Fig. 6. Panel (c) shows the deviation $S_0 - \eta/2\beta$ for 1-step solutions (lower curve), 2-step solutions (middle) to 3-step solutions (upper) for the case in panel (b). Plot (c) shows that S_0 for 1-step structures is always very close $\eta/2\beta$. We use this fact later when we construct approximations for 1-step solutions.

$\cos(\pi kx/L)$. One-step solutions either are stable right from η_1 (supercritical bifurcation) or from a slightly smaller η after secondary saddle-node bifurcation. In all our numerical experiments it remained stable. Multistep solutions are always born unstable, and we did not observe bifurcations which could make them stable for other η. This explains why multistep solutions do not persist.

But the ultra-long duration of transients is still unexplained. This may be related to very weak instability of developed multistep solutions. We study their stability with the help of approximate and numerical techniques.

3.4. Stability of Stationary Solutions—Numerical Results

Since we can obtain stationary solutions $u(x)$, $S(x)$ numerically, we can linearize the original equations in their vicinity and study the dynamics of small perturbations. To enhance accuracy we change the variables in the system. As it can be seen from Fig. 8, $u(x,t)$ has much steeper transitions than $S(x,t)$ and hence on the same grid it diminishes the accuracy of numerical approximations. For this purpose we introduce a new variable $z(x,t)$ such that

$$u(x,t) = \frac{1}{1+e^{-z(x,t)}}, \tag{25}$$

then for stationary structures $z(x) = S(x) - S_0$. The derivatives $u_x = u(1-u)z_x$, $u_t = u(1-u)z_t$, and the Eqs. (5) and (6) become

$$z_t = D_1 (z_{xx} - S_{xx}) - D_1 \tanh \frac{z}{2} z_x (z_x - S_x), \tag{26}$$

$$S_t = D_2 S_{xx} + \frac{\eta}{2} \left(1 + \tanh \frac{z}{2}\right) - \beta S. \tag{27}$$

Here we use

$$1 - 2u = -\frac{1-e^{-z}}{1+e^{-z}} = -\tanh \frac{z}{2}, \qquad \frac{1}{1+e^{-z}} = \frac{e^{z/2}}{e^{z/2}+e^{-z/2}}$$
$$= \frac{\sinh(z/2)+\cosh(z/2)}{2\cosh(z/2)} = \frac{1}{2}\left(1+\tanh \frac{z}{2}\right).$$

Substituting $z(x,t) = z(x) + \delta z(x,t)$, $S(x,t) = S(x) + \delta S(x,t)$ and linearizing equations we obtain

$$\delta z_t = D_1 (\delta z_{xx} - \delta S_{xx}) - D_1 \tanh \frac{z}{2} z_x (\delta z_x - \delta S_x), \tag{28}$$

$$\delta S_t = D_2 \delta S_{xx} + \frac{\eta}{4 \left(\cosh \frac{z}{2}\right)^2} \delta z - \beta \delta S. \tag{29}$$

Here we use $z_x - S_x = 0$, and hence the variation of $\tanh(z/2)z_x$ vanishes. These equations do not contain derivatives of u and we can expect better accuracy of numerical results.
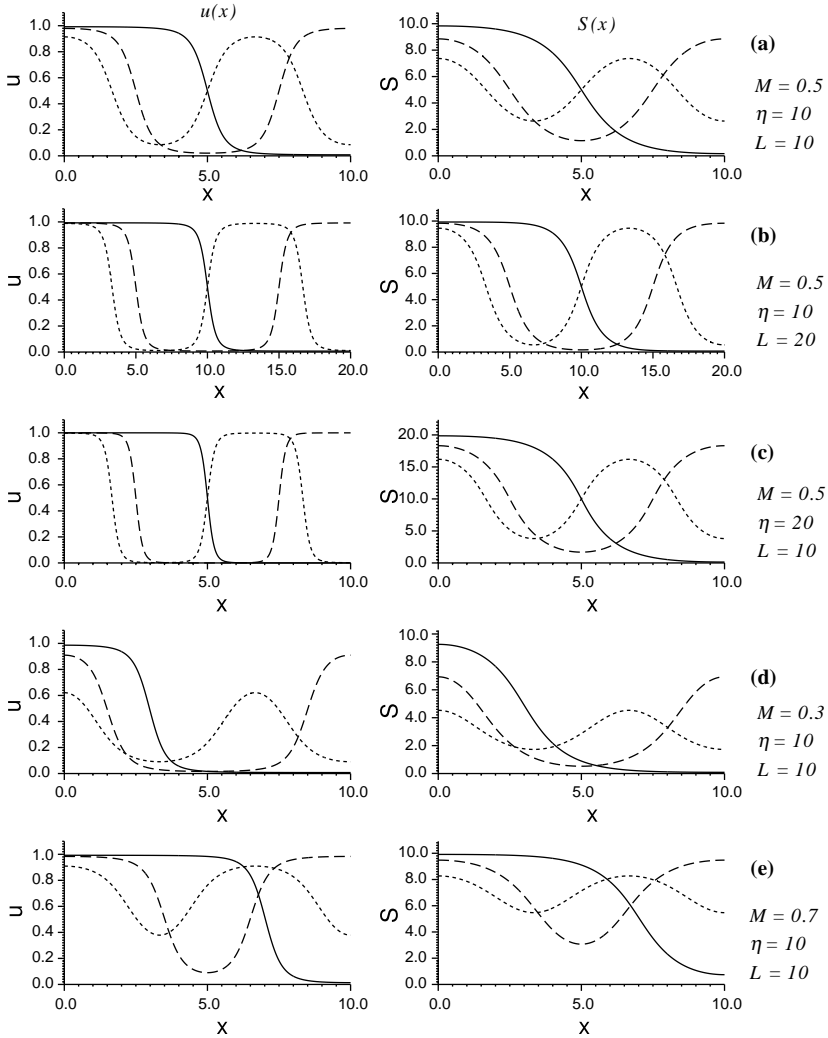
Figure 8. Examples of stationary profiles $u(x)$ (left) and $S(x)$ (right), with one-step (solid), two-step (long dash), and three-step (short dash) for varying parameters, (a)–(e) with fixed $D_2 = \beta = 1$. There are two kinds of two-step (and all other even-step) solutions: with maxima or minima at the boundaries. Only solutions with maxima at the boundaries are shown. When $M \neq 1/2$, these two kinds of solutions usually have different instabilities (see below).

Substituting $\delta z(x,t) = \delta z(x)e^{vt}$, $\delta S(x,t) = \delta S(x)e^{vt}$ we obtain the eigenvalue problem

$$v\delta z = D_1 (\delta z_{xx} - \delta S_{xx}) - D_1 \tanh \frac{z}{2} z_x (\delta z_x - \delta S_x), \tag{30}$$

$$v\delta S = D_2 \delta S_{xx} + \frac{\eta}{4 (\cosh(z/2))^2} \delta z - \beta \delta S \tag{31}$$

with the boundary conditions $\delta z_x(0) = \delta z_x(L) = \delta S_x(0) = \delta S_x(L) = 0$. We solve it numerically for a number of stationary profiles $S(x)$.

Figure 9 shows the profiles of the solutions and the first five eigenfunctions for three stationary solutions. Figure 14 shows the dependence of positive eigenvalues on L: they exponentially approach zero. Numerical results for (28), (29) are in good agreement with the conjecture that the number of positive eigenvalues remains the same along the bifurcation branch.

Figure 9 also shows that the eigenvectors $\delta S_1(x)$ for one-step and two-step solutions are very close to the derivative of the stationary solution S_x. Therefore, the evolution of small perturbations of a stationary two-step profile $S(x)$ should proceed as a synchronous motion of both steps since

$$S(x,t) \approx S(x) + e^{v_1 t} \delta S_1(x) \approx S(x) + ce^{v_1 t} S_x(x) \approx S(x + ce^{v_1 t}),$$

$c \ll 1$.

4. APPROXIMATE STUDY OF LONG TRANSIENTS

4.1. Approximation of Stationary Profiles

To study the long transient solutions we need to understand the dependence of their maximal and minimal values on L. Rigorous estimates could be obtained from the equations of motion, but they contain an unknown parameter S_0. For our purposes it is enough to get an approximate estimate. To get such an estimate we shall use the method of matched asymptotics. We shall build an approximation for a one-step structure only. Multi-step solutions can be approximated by repeating the argument.

To build an approximate solution we follow four steps and use the observations obtained earlier.

Step 1: For a single-step solution far from the bifurcation point η_1, the value of S_0 is very close to $\eta/2\beta$ regardless of the value of M (see Fig. 7). So we shall set $S_0 = \eta/2\beta$.

Step 2: The one-step solution looks like a transient between two almost homogeneous solutions, one of which is close to η/β, the other
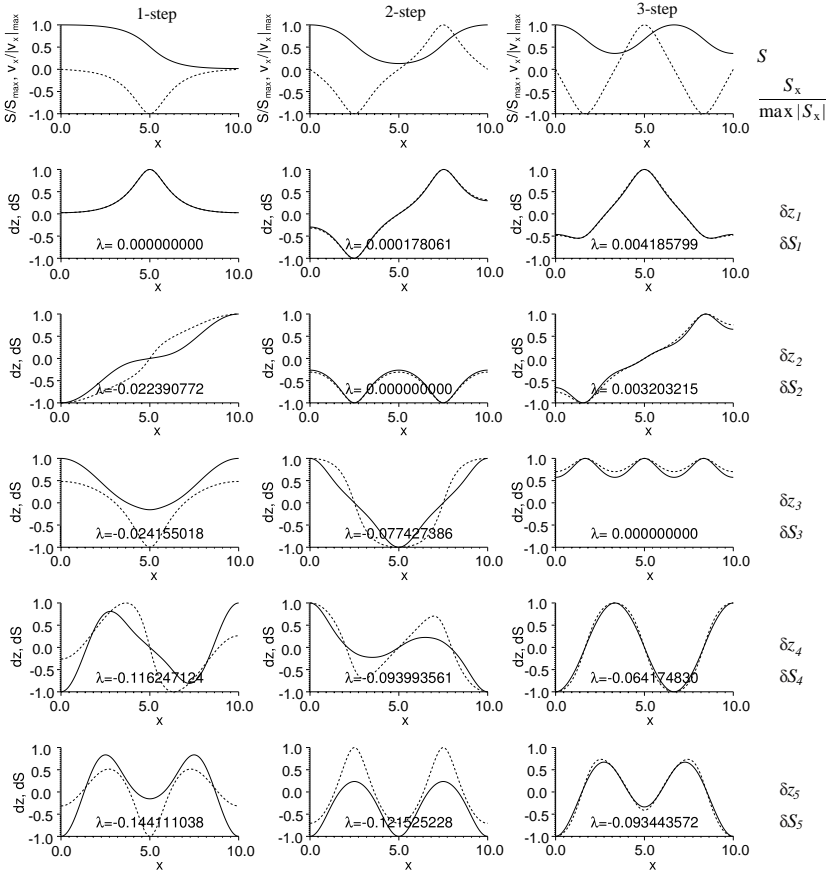
Figure 9. Examples of stationary profiles $S(x)$ and corresponding eigenfunctions δz_k, δS_k for five largest eigenvalues ν_k. It is interesting that $\delta S_1(x)$ for 1-step and 2-step solutions are very close to $S_x(x)$. For the 1-step solution this means that changing M shifts the step left or right. The instability of a 2-step solution results in synchronous motion of both steps in the same direction, that corresponds to a redistribution of u and S under preservation of the shape of the steps.

is close to 0. We denote these two S-levels as S_1 and S_2, respectively. A necessary condition for existence of spatially inhomogeneous solutions is $\eta/2\beta > 2$. We are interested in values of η which are large enough to allow for multistep patterns, hence we assume $e^{-\eta/2\beta} \ll 1$.

Since S_1 and S_2 are close to spatially uniform profiles, they should satisfy

$$\frac{\eta}{1+e^{\eta/2\beta-S_i}} - \beta S_i = 0.$$

There is no analytical solution to this equation, so we use a 0th order approximation

$$S_1 = \frac{\eta}{\beta}, \quad S_2 = 0$$

or the first-order approximation

$$S_1 = \frac{\eta}{\beta} \frac{1}{1 + e^{-\eta/2\beta}} \approx \frac{\eta}{\beta}(1 - e^{-\eta/2\beta}), \tag{32}$$

$$S_2 = \frac{\eta}{\beta} \frac{1}{1 + e^{\eta/2\beta}} \approx \frac{\eta}{\beta} e^{-\eta/2\beta}. \tag{33}$$

Step 3: Let us consider a nonuniform solution $S(x)$. Near S_1 or S_2 its behavior can be approximately described by a linearized equation (19). Let $S = S_i + s_i$, then

$$D_2 s_{ixx} - \beta \left(1 - \frac{\eta e^{S_0 - S_i}}{\beta(1 + e^{S_0 - S_i})^2} \right) s_i = 0. \tag{34}$$

For both S_1, S_2

$$1 - \frac{\eta e^{S_0 - S_i}}{\beta(1 + e^{S_0 - S_i})^2} \approx 1 - \frac{\eta}{\beta} e^{-\eta/2\beta} \approx 1,$$

therefore both s_1 and s_2 satisfy the same equation

$$D_2 s_{ixx} - \beta s_i = 0.$$

For definiteness, let $S(x) \approx S_1$ near the left boundary $(x = 0)$ and $S(x) \approx S_2$ at the right boundary $(x = L)$. Then the solutions satisfying the zero flux condition at the corresponding boundary are

$$s_1 = A \cosh \omega x, \quad s_2 = B \cosh \omega (L - x), \quad \omega = \sqrt{\frac{\beta}{D_2}}. \tag{35}$$

Step 4: Now to get an approximate description of the whole one-step solution let us match together $S_1 + s_1$ and $S_2 + s_2$ (see Fig. 10)

$$S_A(x) = \begin{cases} S_1 + s_1(x), & 0 < x < x_1, \\ S_2 + s_2(x), & x_1 < x < L \end{cases} \tag{36}$$

with the matching conditions at $x = x_1$

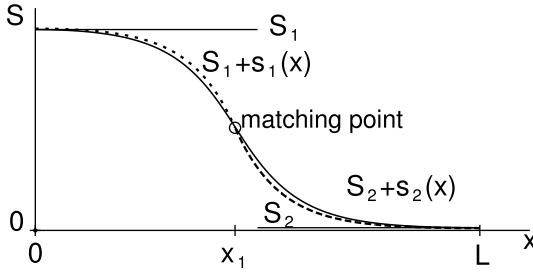$$S_1 + s_1(x_1) = S_2 + s_2(x_1), \quad s_{1x}(x_1) = s_{2x}(x_2) \tag{37}$$

Figure 10.   Scheme of approximation to a 1-step structure.

and the integral condition (20)

$$\frac{1}{L}\int_0^L S_A(x)\mathrm{d}x = \frac{\eta M}{\beta}. \tag{38}$$

These three conditions give the values of A and B and the matching point x_1.

Substituting (35) we obtain from (36) to (38)

$$S_1 + A\cosh\omega x_1 = S_2 + B\cosh\omega(L-x_1),$$
$$\omega A\sinh\omega x_1 = -\omega B\sinh\omega(L-x_1),$$

$$A = -(S_1 - S_2)\frac{\sinh\omega(L-x_1)}{\sinh\omega L}, \qquad B = (S_1 - S_2)\frac{\sinh\omega x_1}{\sinh\omega L}.$$

Now

$$\begin{aligned}
\frac{1}{L}\int_0^L S_A(x)\,\mathrm{d}x &= \frac{1}{L}\int_0^{x_1}(S_1 + A\cosh\omega x)\,\mathrm{d}x + \frac{1}{L}\int_{x_1}^L (S_2 + B\cosh\omega(L-x))\,\mathrm{d}x \\
&= \frac{x_1 S_1 + (L-x_1)S_2}{L} + \frac{1}{\omega L}(A\sinh\omega x_1 + B\sinh\omega(L-x_1)) \\
&= \frac{x_1 S_1 + (L-x_1)S_2}{L} = S_2 + \frac{x_1}{L}(S_1 - S_2) \\
&= \frac{\eta M}{\beta}.
\end{aligned}$$

Substituting the expressions for S_1 and S_2 we obtain

$$e^{-\eta/(2\beta)} + \frac{x_1}{L}\left(1 - 2e^{-\eta/(2\beta)}\right) = M, \qquad x_1 = \vartheta L, \qquad \vartheta = \frac{M - e^{-\eta/(2\beta)}}{1 - 2e^{-\eta/(2\beta)}} \approx M.$$

Finally

$$A = -\frac{\eta}{\beta}(1 - 2e^{-\eta/(2\beta)})\frac{\sinh\omega(1-\vartheta)L}{\sinh\omega L}, \quad B = \frac{\eta}{\beta}(1 - 2e^{-\eta/(2\beta)})\frac{\sinh\omega\vartheta L}{\sinh\omega L}. \tag{39}$$

If we use the first-order approximations as given in (32), (33) we find the following explicit form of the one-step approximation:

$$S_A(x) = \begin{cases} \frac{\eta}{\beta}\frac{1}{1+e^{-\eta/2\beta}} - \frac{\eta}{\beta}\left(1 - 2e^{-\eta/(2\beta)}\right)\frac{\sinh(\omega(1-\vartheta)L)}{\sinh(\omega L)}\cosh(\omega x), & 0 < x < x_1, \\ \frac{\eta}{\beta}\frac{1}{1+e^{\eta/2\beta}} + \frac{\eta}{\beta}\left(1 - 2e^{-\eta/(2\beta)}\right)\frac{\sinh(\omega\vartheta L)}{\sinh(\omega L)}\cosh(\omega(L-x)), & x_1 < x < L. \end{cases} \tag{40}$$

Figure 11 compares approximate solutions with numerical steady states. Experiments show that the agreement is good when L is essentially greater than the size of the transition layer, and M is not too close to 0 or 1. Figure 12 compares the dependence on L for A, B, and their estimates from the numerically obtained profiles:

$$\tilde{A} = \frac{S(x) - S(0)}{\cosh(\omega x) - 1}, \quad x \approx 0, \qquad \tilde{B} = \frac{S(x) - S(L)}{\cosh(\omega(L-x)) - 1}, \quad x \approx L.$$

It is essential that the approximations capture the exponential dependence on L.

Note. The constructed approximate solution has only C^1 smoothness. It is possible to suggest a C^2 approximation by matching three linearized solutions, $S_1 + s_1$, $\eta M/\beta + s_m$, and $S_2 + s_2$, where s_m is a linearization about the unstable spatially uniform solution. However, this approximation leads to analytically intractable formulas.

4.2. Two-Step Structure: the Mechanism of Slow Decay

Let us consider the following situation. From initial data quick transient processes have prepared a two-step pattern with the maxima at the boundaries and one minimum in the middle. This pattern can be considered as consisting of two one-step structures with the lengths L_1 and L_2, such that both of them have the same mean M as the initial data. For definiteness, let $L_1 < L_2$. For each of the step structures the deviation from the trivial solution is given by A or B in formula (39). The dependence on L is given through the ratio

$$\frac{\sinh(\omega(1-\vartheta)L)}{\sinh(\omega L)} \approx e^{-\vartheta L}$$

for L large enough. Hence it is decreasing in L, which means that steps with unequal lengths $L_1 < L_2$ cannot be matched perfectly. Upward or
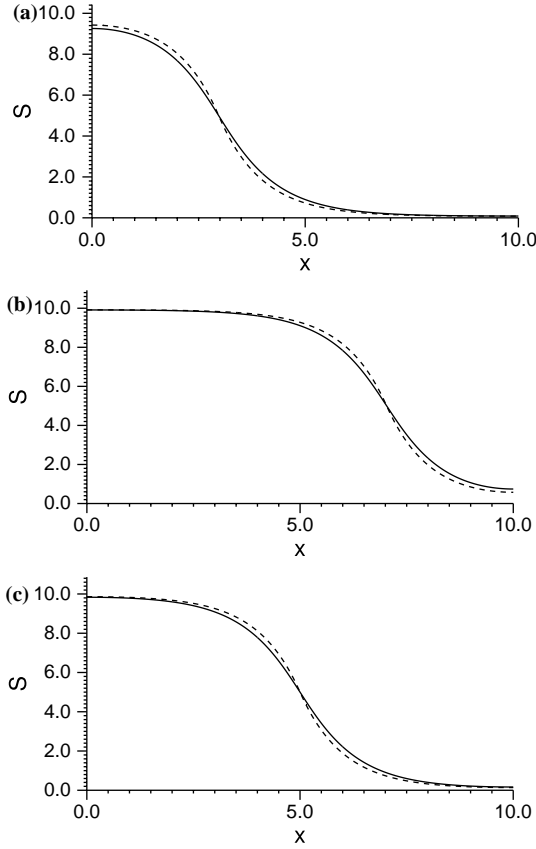
Figure 11. Examples of approximations (dashed line) and steady state (solid line) for the 1-step stationary solutions for $M = 0.3$ (a), 0.5 (b) and 0.7 (c), $D_2 = \beta = 1$, $\eta = 10$, $L = 10$.

downward connections are shown in Fig. 13. Due to this mismatch a small gradient emerges and the corresponding flow drives particles from the short structure to the long one. As a result the short structure becomes shorter and eventually collapses while the long one becomes longer until it occupies the whole domain $L = L_1 + L_2$.

Let us construct approximate quantitative estimates from this scenario. We shall use the following additional assumptions.

(A1)   The shape of both structures is almost stationary at all times, and hence their properties are entirely defined by their lengths L_i via (40).

(A2)   The relaxation of the concentration of attractant S is faster than the relaxation of the particles u, so we assume that pointwise $S \approx \eta u / \beta$.
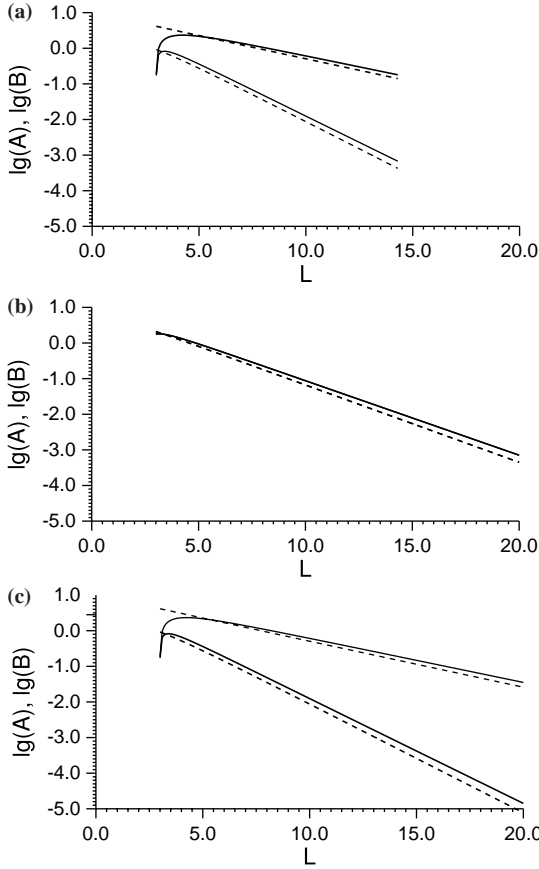
Figure 12. Dependence on L of the coefficients $|A|$ (thick dash), $|B|$ (thin dash) for approximations (39) and their estimates $|\tilde{A}|$, $|\tilde{B}|$ from numerically obtained $S(x)$ (solid lines). $M = 0.3$ (a), 0.5 (b) and 0.7 (c), $D_2 = \beta = 1$, $\eta = 10$. Exponential dependence is clearly visible, and it is captured by the approximations.

4.2.1. B-Pattern

Now we study two-step solutions which are joined at the bottom (B-type). In the well between the steps, S is small and u is even smaller: $S \sim S_2 \sim (\eta/\beta)e^{-\eta/2\beta}$, $u \sim 1/(1 + e^{S_0}) \approx e^{-S_0} = e^{-\eta/2\beta}$. Therefore the diffusion flow of the particles $-D_1 u_x$ can be compensated by the chemotactic flow $D_1 u(1-u)S_x$ only if $|u_x| \approx u|S_x| \ll |S_x|$. If the gradients of both particles and attractant are of the same order of magnitude, diffusion beats chemotaxis and the latter is negligible.
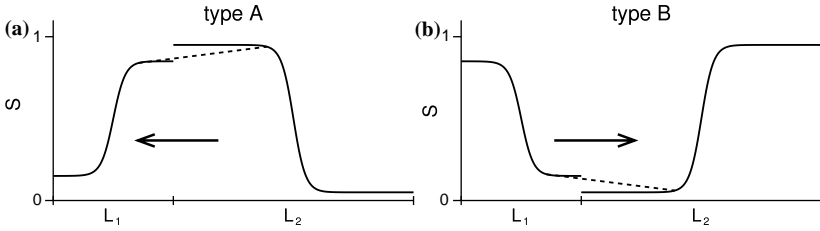
Figure 13. Approximations of two-step patterns, where the steps have unequal lengths. The arrows indicate the direction of diffusional flow along the interface due to arising gradient (dashed line). We call (a) **A-type** and (b) **B-type**. The dotted line indicates a small gradient between the steps, which we use to approximate the particle flux.

For the estimates of the mismatch between the individual steps we can use the approximate relations (39): the lower end of the stationary structure corresponds to the value

$$S_{\min}(L) = S_2 + B \approx \frac{\eta}{\beta} e^{-\eta/2\beta} + \frac{\eta}{\beta} \frac{\sinh \omega \vartheta L}{\sinh \omega L} \approx \frac{\eta}{\beta} e^{-\eta/2\beta} + \frac{\eta}{\beta} e^{-\omega(1-M)L},$$

therefore the mismatch is

$$M_S = S_{\min}(L_1) - S_{\min}(L_2) \approx \frac{\eta}{\beta}(e^{-\omega(1-M)L_1} - e^{-\omega(1-M)L_2}).$$

For stationary structures we have the relation (17), hence the corresponding mismatch in u is

$$M_u = \varphi\left(S_{\min}(L_1)\right) - \varphi\left(S_{\min}(L_2)\right) \approx \varphi'\left(\overline{S_{\min}}\right) M_S \approx u M_S.$$

This mismatch leads to a small gradient of u over the well bottom. The size of the transition layer corresponds to $(1-M)(L_1+L_2)$ hence we find a flux of the order of magnitude

$$w = D_1|u_x| \sim \frac{D_1 M_u}{(1-M)(L_1+L_2)} \approx D_1 \frac{\eta}{\beta} \frac{e^{-\eta/2\beta}}{(1-M)L}(e^{-\omega(1-M)L_1} - e^{-\omega(1-M)L_2}).$$

During a small time interval dt this flow transfers the amount of particles from left to right $du \sim w dt$. Since we assume that the shape of the steps remain stationary, this transfer causes the shift of both steps to the left, so both L_1 and L_2 change. Since the content of particles in each structure is LM, $du = M dL$. Then we come to the equations $dL_1/dt = -(w/M)$, $dL_2/dt = w/M$. Let us introduce the new variable

$\zeta = L_2 - L_1$, then $2L_2 = L + \zeta$, $2L_1 = L - \zeta$. An equation for ζ is derived

$$
\begin{aligned}
\frac{d\zeta}{dt} &= \frac{2w}{M} = \frac{2D_1\eta}{\beta M} \frac{e^{-\eta/2\beta}}{(1-M)L} e^{-\omega(1-M)(L/2)} (e^{\omega(1-M)\frac{\zeta}{2}} - e^{-\omega(1-M)\frac{\zeta}{2}}) \\
&= \frac{2\gamma_B}{\omega(1-M)} \sinh \frac{\omega(1-M)\zeta}{2}.
\end{aligned}
$$

This equation has one unstable fixed point at zero, and its eigenvalue γ_B gives the estimate of the principal eigenvalue for the two-step stationary structure,

$$
\gamma_B = \frac{2\omega D_1\eta}{\beta ML} e^{-\omega(1-M)\frac{L}{2} - \frac{\eta}{2\beta}}, \qquad \omega = \sqrt{\frac{\beta}{D_2}}. \tag{41}
$$

We shall call this pattern a B-type pattern because of the mismatch at the bottom level described by the coefficient B.

4.2.2. A-Patterns

Similarly it is possible to consider the A-type pattern (Fig. 13) with a maximum in the middle and two minima at the boundaries. The mismatch will depend on the parameter A and the corresponding estimate for the eigenvalue is

$$
\gamma_A = \frac{2\omega D_1\eta}{\beta(1-M)L} e^{-\omega M(L/2)-(\eta/2\beta)}. \tag{42}
$$

So, we have $\gamma_A \neq \gamma_B$ if $M \neq \frac{1}{2}$. Note that the formulas for γ_A and γ_B are equivalent if we replace M by $1 - M$ (see Lemma 1.1).

4.2.3. A- and B-Patterns: Merging and Dissolving

The difference in decay rates of two configurations shown in Fig. 13 arises because they correspond to two different processes. It is natural to interpret a maximum of the particle concentration as a particle aggregate—a "swarm". The zero flux conditions at the boundary can be interpreted such that the profiles of u and S are symmetrically extended beyond the boundary. If we reflect the profiles about the point $x = 0$, we can see that an A-pattern corresponds to two equal swarms moving towards each other and merging. The B-pattern corresponds to a small swarm between two large ones, the large swarms are slowly pumping the particles out of the small one until it dissolves completely. Therefore it is not surprising that the two different processes have different characteristic speeds.

On the other hand, we have seen in Lemma 1.1 that the original system is symmetric w.r.t. $M = 1/2$. Indeed, if we replace $(1 - M)$ by M in
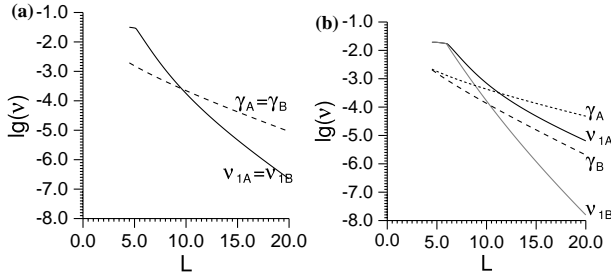
Figure 14. Examples of dependence of positive eigenvalues ν on L for 2-step solutions (a,b). $D_1 = 0.1$, $D_2 = \beta = 1$, $\eta = 10$, $M = 0.5$ (a), 0.3 (b). The dashed lines correspond to γ_A (short dash) and γ_B (long dash), where γ_A and γ_B are the unstable eigenvalues of the approximations as given by formula (41) and (42) for A- and B-pattern, respectively. The values ν_{1A} and ν_{1B} are the numerically calculated leading eigenvalues of the eigenvalue problem (30, 31) for A- or B-pattern, respectively.

either of the formulas (41) or (50) then we obtain the corresponding formulas for the B-pattern, (42), (52), respectively.

The evolution of the chemotactic structures typically is a sequence of such mergings and dissolvings. For instance, the evolution of the five-step structure in Fig. 1 proceeds as follows: first the swarm at the right boundary dissolves, then two swarms merge in the middle, and finally the resulting single swarm merges with its counterpart beyond the right boundary. Therefore both merging and dissolving is important for the evolution.

Note that (41) and (42) involve exponential dependence on L, which qualitatively agrees with the numerical data, Fig. 14. This explains the observed substantial slowing down of the decay processes. As we can see in Fig. 1 or Fig. 1 in [6], a complex structure can be considered as a number of two-step patterns of A or B type, and usually one of the combinations evolves faster than other. As the number of steps decreases, the lengths of the two-step combinations increase, which may cause significant decrease in the evolution speed.

4.2.4. Stability of Two-Step Steady States

Here we study the stability of two-step steady states. For large L we find an exponentially small unstable leading eigenvalue. The approximation used here is based on ideas which were developed in context of microwave heating in [9].

We consider the eigenvalue problem (30), (31) for both types of two-step structures and approximate the leading eigenvalue ν_1. The unknown functions δz and δS are the perturbations of the steady state.

We use a number of simplifying assumptions, which are supported by numerical data.

1. We approximate a two-step stationary solution by two approximate one-step solutions $S_A(x)$ on the domain $L/2$.
2. We assume that for the slowly evolving perturbed stationary profile approximately $u(x) + \delta u(x, t) \approx \varphi(S(x) + \delta S(x, t))$, where φ is defined in (17), that is $\delta z_1(x, t) \approx \delta S_1(x, t)$. Let us denote the difference by $\delta w = \delta z_1 - \delta S_1$, then we assume that $|\delta w| \ll |\delta S_1|$.
3. In the following analysis we will work with u and z simultaneously, they are related by (25). For stationary profiles $u(x)$, $z(x)$, and $S(x)$ we have the relations

$$\alpha(x) \equiv \frac{1}{4\left(\cosh(z(x)/2)\right)^2} = u(1-u),$$

$$u_x = u(1-u)S_x.$$

Then Eqs. (30) and (31) can be written as

$$\nu\delta w + \nu\delta S = \frac{D_1}{u(1-u)}\left(u(1-u)\delta w_x\right)_x, \tag{43}$$

$$\nu\delta S = D_2\delta S_{xx} + \eta\alpha(x)\delta z - \beta\delta S. \tag{44}$$

4. The domain length L is assumed to be large enough. Below we shall specify this assumption in more detail.
5. We observe numerically in Fig. 9 that the profile of the leading eigenfunction $\delta S_1(x)$ is very close to S_x except near the boundaries, since $\delta S_x|_{x=0,L} = 0$ and $S_{xx}|_{x=0,L} \neq 0$ (Fig. 9). We describe this with a boundary layer approximation

$$\delta S_1(x) \approx S_x(x) + S_L(x) + S_R(x), \tag{45}$$

where S_L and S_R describe the boundary layers at the left and right boundary respectively. We assume that S_L is $O(1)$ only near the left boundary $x = 0$, where $S_x \approx 0$, and outside this domain $S_L \approx 0$. The same is true about S_R near $x = L$. In other words, we assume

$$S_L(L) = 0, \quad S_R(0) = 0, \qquad S_x S_L \approx S_x S_R \approx 0.$$

Near the boundaries $S(x)$ is close to one of the levels S_1 or S_2 (32), (33), and in both cases $\eta\alpha(x) = \eta u(1-u) \ll 1$. Hence

$$D_2 S_{Lxx} - \beta S_L = 0, \qquad D_2 S_{Rxx} - \beta S_R = 0,$$

with the boundary conditions

$$S_{xx}(0) + S_{Lx}(0) = 0, \qquad S_{xx}(L) + S_{Rx}(L) = 0.$$

This gives

$$S_L(x) = \frac{1}{\omega} S_{xx}(0) e^{-\omega x}, \quad S_R(x) = -\frac{1}{\omega} S_{xx}(L) e^{-\omega(L-x)}, \quad \omega^2 = \frac{\beta}{D_2}.$$

6. Note that the stationary two-step solutions are symmetric, hence $S(L) = S(0)$, $S_{xx}(L) = S_{xx}(0)$.

Below we omit the index 1 for δS_1, ν_1, δz_1.

We can neglect the term $\nu \delta w$ in (43), then we obtain the equation for δw

$$
\begin{aligned}
(u(1-u)\delta w_x)_x &= \frac{\nu}{D_1} u(1-u)\delta S = \frac{\nu}{D_1} u(1-u) \left(S_x + S_L + S_R \right) \\
&\approx \frac{\nu}{D_1} u(1-u) S_x = \frac{\nu}{D_1} u_x.
\end{aligned}
$$

Here we use the fact that in the domain where the boundary layer functions S_L, S_R are essentially nonzero the term $u(1-u) \approx 0$ and vice versa. The boundary conditions for δw are the same as for δz and δS, $\delta w_x(0) = \delta w_x(L) = 0$. Now

$$u(1-u)\delta w_x = \frac{\nu}{D_1} (u(x) - u(0)). \tag{46}$$

Equation (44) gives

$$\nu \delta S = D_2 \delta S_{xx} + \eta \alpha(x) \delta S + \eta \alpha(x) \delta w - \beta \delta S.$$

Since $\delta w \sim \nu$, let us move the term $\eta \alpha(x)\delta w$ to the left-hand side,

$$\nu \delta S - \eta \alpha(x) \delta w = D_2 \delta S_{xx} + \eta \alpha(x) \delta S - \beta \delta S \equiv A \delta S,$$

multiply it by S_x and integrate from 0 to L. This gives

$$\nu \int_0^L S_x \left(S_x + S_L + S_R \right) dx + \eta \int_0^L S_x u(1-u)\delta w \, dx = \int_0^L S_x \left(A \delta S \right) dx. \tag{47}$$

Simplifying and integrating by parts we obtain

$$
\begin{aligned}
\eta \int_0^L S_x u(1-u)\delta w \, dx = \eta \int_0^L u_x \delta w \, dx &= \eta u \delta w |_0^L - \eta \int_0^L u \delta w_x \\
&= \eta u(0) \left(\delta w(L) - \delta w(0) \right) - \eta \int_0^L \frac{\nu}{(1-u)D_1} (u - u(0)) \, dx.
\end{aligned}
$$

From (46) it follows that

$$\delta w(L) - \delta w(0) = \frac{v}{D_1} \int_0^L \frac{u - u(0)}{u(1-u)} dx,$$

hence

$$\eta \int_0^L S_x u(1-u) \delta w \, dx = -\frac{\eta v}{D_1} \int_0^L \frac{(u - u(0))^2}{u(1-u)} dx.$$

The term $S_x (S_L(x) + S_R(x)) \approx 0$, at the boundary $S_x = 0$, far from the boundary $S_{L,R} \approx 0$, hence

$$v \int_0^L S_x (S_x + S_L + S_R) \, dx \approx v \int_0^L S_x^2 \, dx.$$

Finally, integrating by part the right hand side of (47) one has

$$\int_0^L S_x (A \delta S) \, dx = D_2 S_x \delta S_x |_0^L - D_2 S_{xx} \delta S |_0^L + \int_0^L \delta S (A S_x) \, dx = - D_2 S_{xx} \delta S |_0^L.$$

Since $S(x)$ is the stationary profile, differentiating (19) we have $A S_x = 0$, therefore $\int_0^L \delta S (A S_x) \, dx = 0$. Taking into account the relations for S_L and S_R and symmetry of the $S(x)$ profile, we have

$$-D_2 S_{xx} \delta S |_0^L = D_2 S_{xx}(0) S_L(0) - D_2 S_{xx}(L) S_R(L)$$
$$= \frac{D_2}{\omega} (S_{xx}(0))^2 + \frac{D_2}{\omega} (S_{xx}(L))^2 = \frac{2 D_2}{\omega} (S_{xx}(0))^2.$$

Combining it all we obtain the relation for estimating the leading eigenvalue v:

$$v \left(\int_0^L S_x^2 \, dx + \frac{\eta}{D_1} \int_0^L \frac{(u - u(0))^2}{u(1-u)} dx \right) = \frac{2 D_2}{\omega} (S_{xx}(0))^2.$$

Due to symmetry of two-step solutions, $S(x) = S(L - x)$ it is sufficient to integrate from 0 to $L/2$,

$$v \left(\int_0^{L/2} S_x^2 \, dx + \frac{\eta}{D_1} \int_0^{L/2} \frac{(u - u(0))^2}{u(1-u)} dx \right) = \frac{D_2}{\omega} (S_{xx}(0))^2. \tag{48}$$

Half of the two-step structure can be replaced by approximate one-step solution on the domain $L/2$. Again there are two types of two-step structures.

A-pattern: Minimum at the boundary, maximum at the center.

$$S(x) \approx \begin{cases} S_2 + B \cosh \omega x, & x < x_M, \\ S_1 + A \cosh \omega \left(\frac{L}{2} - x \right), & x > x_M, \end{cases} \quad x_M \approx (1 - M) \frac{L}{2} \tag{49}$$

$$A \approx -S_1 \frac{\sinh M\omega \frac{L}{2}}{\sinh \omega \frac{L}{2}} \approx -S_1 \exp\left(-(1-M)\,\omega \frac{L}{2}\right),$$

$$B \approx S_1 \frac{\sinh(1-M)\,\omega \frac{L}{2}}{\sinh \omega \frac{L}{2}} \approx S_1 \exp\left(-M\omega \frac{L}{2}\right).$$

For this solution we need to find good approximations for the terms in (48). Here we use the fact that L is large and we study asymptotic expansions. The details are given in Appendix A. We denote the approximative leading eigenvalue for an A-pattern by γ_{1A}. We find (see Appendix A)

$$\gamma_{1A} \approx \frac{2D_1\eta}{ML} \exp\left(-\omega ML - \frac{\eta}{2\beta}\right), \tag{50}$$

which is exponentially small for large L.

B-pattern: Minimum at the center, maximum at the boundary.

$$S(x) \approx \begin{cases} S_1 + A\cosh \omega x, & x < x_M, \\ S_2 + B\cosh \omega\left(\frac{L}{2} - x\right), & x > x_M, \end{cases} \qquad x_M \approx M\frac{L}{2} \tag{51}$$

with the same A and B as above.

Again, the asymptotic expansions are shown in Appendix A. We find an approximative eigenvalue for a B-pattern

$$\gamma_{1B} \approx \frac{2D_1\eta}{(1-M)L} \exp\left(-\omega(1-M)L - \frac{\eta}{2\beta}\right). \tag{52}$$

In Fig. 15 we compare the approximative eigenvalues γ_{1A}, γ_{1B} with the numerically obtained eigenvalues. We see that the approximations (50) and (52) show the correct slope as functions of L, in contrast to the approximation done earlier in (41) and (42), and shown in Fig. 14. If we compare the formulas for the approximate eigenvalues for A-patterns (50) and (41) and for B-patterns (52) and (42) we find a very similar dependence in the exponent. In the first case the exponent has a factor $L/2$, which is L in the second case. In all cases the factor in front of the exponential of the eigenvalue is proportional to D_1 and η and inversely proportional to L.
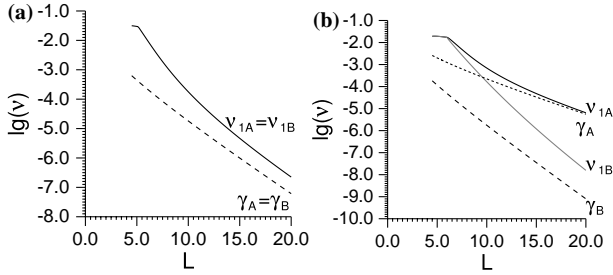
Figure 15. Examples of dependence of positive eigenvalues ν on L for 2-step solutions (a,b). $D_1 = 0.1$, $D_2 = \beta = 1$, $\eta = 10$, $M = 0.5$ (a), 0.3 (b). The dashed lines correspond to modified estimates of γ_A (short dash) and γ_B (long dash), where γ_A and γ_B are the unstable eigenvalues of the approximations as given by formula (50) and (52) for A- and B-pattern, respectively. The values ν_{1A} and ν_{1B} are the numerically calculated leading eigenvalues of the eigenvalue problem (30, 31) for A- or B-pattern, respectively.

5. OTHER MODELS WITH PSEUDOSTRUCTURES

Note that the qualitative explanation of the ultra-long transients in the previous section does not essentially use the specific dependence of the chemotactic coefficient on u and S in (2). The same explanation involving small gradients due to the mismatch of the individual one-steps may be valid for other types of $\chi(u, S)$. The most important is the nature of the interaction between simple structures combined with particle conservation—increase of the particle content in one structure implies decrease of particle content in the other structure. Therefore we looked for the effect of pseudostructures in other models and indeed found them.

Similar metastable structures were observed in models for microwave heating [9], Cahn–Hilliard structures [5] and many other examples.

To obtain other models with pseudostructures we take system (26), (27) and neglect the term containing $\tanh(z/2)z_x$. We introduce $w = z - S$, $S = z - w$, then we get

$$z_t = D_1 w_{xx}, \tag{53}$$

$$z_t - w_t = D_2 z_{xx} - D_2 w_{xx} + \frac{\eta}{2}\left(1 + \tanh\frac{z}{2}\right) - \beta z + \beta w. \tag{54}$$

We differentiate the second equation twice by x, multiply it by D_1 and substitute $D_1 w_{xx} = z_t$ from the first equation. This gives

$$D_1 z_{xxt} - z_t = D_1 D_2 z_{xxxx} - D_2 z_{xxt} + D_1\frac{\eta}{2}\left(\tanh\frac{z}{2}\right)_{xx} - D_1\beta z_{xx} + \beta z_t$$

or

$$(1+\beta)z_t = \left(-D_1 D_2 z_{xx} - \frac{1}{2}D_1\eta\left(\tanh\frac{z}{2}\right) + D_1\beta z + D_2 z_t \right)_{xx}. \quad (55)$$

This is the so-called viscous Cahn–Hilliard equation. Here the conserved quantity is z, its stationary solutions are almost the same as for the chemotaxis model (they differ by a constant) and as in the chemotaxis model there are rigorous results, that only monotonous spatially inhomogeneous stationary solution can be stable [5]. We observed the effect of pseudo-structures in this equation as well, though the transition times were less and the eigenvalues for stationary solutions were larger.

The above Cahn–Hilliard equation, without the viscuous damping term z_{txx}, appears as a gradient flow in H^{-1} of the energy functional

$$J(z) = \int \left(\frac{D_1 D_2}{2}|z_x|^2 - \eta D_1 \ln(\cosh(z/2)) + \frac{D_1\beta}{2}z^2 \right) dx$$

which is a double-well potential when η/β is large enough.

Metastability for the viscous Cahn–Hilliard equation was studied by Sun and Ward [16]. For multistep structures the individual transition layers were parameterized by their locations $x_i(t)$ and a system of ordinary differential equations for the $x_i(t)$ coupled to an algebraic equation (mass conservation) was derived which describes the movement of the transition layers. Indeed, this approach appears to be the next step in the analysis of multi-peak dynamics of the chemotaxis models studied here. In fact, recently Dolak and Schmeiser [4] have carried this out for the above chemotaxis model for small diffusion D_1 and an elliptic equation for S.

Another example of a model with pseudostructures is the classical Keller–Segel model in one spatial dimension, where χ does not depend on u at all.

$$u_t = D_1 u_{xx} - \chi\,(u S_x)_x,$$
$$S_t = D_2 S_{xx} + \alpha u - \beta S,$$
$$0 < x < L,$$
$$u_x|_{x=0,L} = S_x|_{x=0,L} = 0.$$
$$u(x,0) = u_I(x),\ S(x,0) = S_I(x).$$

By varying model parameters it is possible to obtain very long transients. In Fig. 16 we show a typical example.
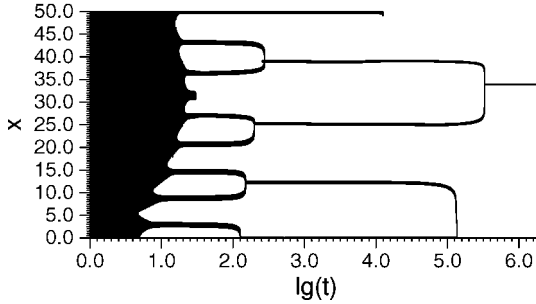
Figure 16. Metastable behavior in the standard Keller–Segel model in one dimension for $D_1 = D_2 = \chi = \alpha = \beta = 1$, $L = 50$, $M = 4$. The initial data are a small perturbation of the homogeneous solution. The picture shows the interaction of peaks of the density u on a logarithmic time scale. The density u is shown black if $u > 2$ and white if $u < 2$. After 10^6 time units all particles aggregate to 2 narrow peaks, at $x = 0$ and $x \approx 33$.

In Sleeman *et al.* [15] the following chemotaxis model on a bounded domain Ω has been studied:

$$u_t = \nabla \left(u \nabla \left(\ln \frac{u}{S^p} \right) \right),$$

$$S_t = \varepsilon^2 \Delta S - S + \frac{uS}{1 + \gamma S},$$

$$\frac{\partial u}{\partial n} = \frac{\partial S}{\partial n} = 0, \quad x \in \partial \Omega$$

with $p > 1$ and $\gamma > 0$. Typical solutions to this model develop sharp spikes, in contrast to the plateau-like patterns of the model studied here. Similar to the model studied here, the corresponding steady states are unstable with exponentially small eigenvalue (metastable). Sleeman *et al.* [16] show that a stable boundary spike will be located at points of the boundary with maximal curvature, and that a stable interior spike has maximum distance to the boundary.

6. CONCLUSIONS

We conclude that the main reason for the formation of pseudostructures is the tradeoff between localized "steps" which resemble stationary patterns in bistable systems and diffusion which does not allow the sub-patterns to be completely independent. It turns out that the properties of the reaction-diffusion equation for S coupled to the equation for a conserved quantity u behaves qualitatively similar to a single reaction diffusion equation. This is probably due to the fact the stationary

solutions are described by a single equation for S, and hence evolution attracts trajectories to the manifold where $u = \varphi(S)$.

It is very interesting to study the various instability conditions of this paper in terms of the parameters of the original model (3). From linearization at the homogeneous steady state we found in formula (9) that all unstable modes k satisfy

$$0 < \left(\frac{\pi k}{L}\right)^2 < \frac{\alpha \chi M(1-M) - D_1 \beta}{D_1 D_2},$$

where M is the mean u value. Pattern formation will not happen for M close to 0 or close to 1. For instabilities to occur α and χ need to be large and β must be small. In addition, strong diffusion would prevent pattern formation.

The most unstable eigenmode is $k = L\sqrt{\mu_U}/\pi$ where μ_U satisfies (10) which in original parameters reads

$$\mu_U > \frac{\alpha M(1-M) - D_1 \beta}{\sqrt{D_1 D_2}(\sqrt{D_1} + \sqrt{D_2})^2}.$$

Large values of α or χ support higher modes (solutions with more peaks), while higher values for D_1 and D_2 support broader plateaus.

Next we look at the approximate transition times of an A or a B pattern. If γ_{1B} denotes the prinicpal eigenvalue of a B-pattern then $T_B = \gamma_{1B}^{-1}$ is the typical time that the solution spends near the corresponding metastable steady state. From (52) we find that approximately

$$T_B \approx \frac{(1-M)L}{2\alpha\chi} \exp\left(\sqrt{\frac{\beta}{D_2}}(1-M)L + \frac{\alpha\chi}{2\beta D_1}\right), \qquad (56)$$

$$T_A \approx \frac{ML}{2\alpha\chi} \exp\left(\sqrt{\frac{\beta}{D_2}}ML + \frac{\alpha\chi}{2\beta D_1}\right). \qquad (57)$$

We see that the transition times strongly depend on diffusion. If $D_1 \to 0$ or $D_2 \to 0$ then $T_A, T_B \to \infty$ and no transitions would occur. A fact that has been shown in the meantime by Dolak and Schmeiser [4].

If only D_1 is small (and D_2 is of order one), then the $\alpha\chi/(2\beta D_1)$-term dominates and the exponent is independent of the length L and the value of M. If, on the other hand, D_2 is small (and D_1 of order one), then α and χ have no influence on the exponent.

We can use T_A and T_B also to study multiple peak transitions. In that case we need to choose appropriate sub-intervals such that in each subinterval we have a single A or B pattern. See for example Fig. 1. Between times $t = 233$ and $t = 5769$ we have a B-pattern transition in the

subinterval [13, 20]. Between $t = 1065$ and $t = 6515$ we obtain a B-pattern transition in [4.5, 13]. And finally for $t > 6515$ we observe an A-pattern transition on the whole domain. To use formulas (57) and (56) the length L has to be replaced by the length of the corresponding subinterval. This explains nicely why patterns with many peaks interact much faster than patterns with only a few peaks.

From viewpoint of applications the metastable patterns are the patterns seen in experiments. In Dolak and Hillen [3] a Cattaneo-based volume filling model has been applied to patterns of *Dictyostelium discoideum* and to patterns of *Salmonella typhimurium*. For Dictyostelium, typical experiments run on time scales of one or two days. During that time a first metastable pattern has formed and a number of transitions can be seen (see experiments of the Firtel-Lab at the University of California, San Diego). The very long transition times for large plateaus are not relevant to the experiments. On the time scale of Dictyostelium the transition to a limit formation would require about 20 years.

ACKNOWLEDGMENTS

APPENDIX A. ASYMPTOTICS

A.1. A-pattern

For the A-pattern given by (49) we find the following asymptotics:

$$
S_{xx}(0) \approx \omega^2 B \approx \omega^2 S_1 \exp\left(-M\omega \frac{L}{2}\right),
$$

$$
\int_0^{L/2} S_x^2 \, dx \approx \int_0^{L/2} S_{Ax}^2 \, dx = \omega^2 B^2 \int_0^{x_M} \sinh^2 \omega x \, dx
$$

$$
+ \omega^2 A^2 \int_{x_M}^{L/2} \sinh^2 \omega \left(\frac{L}{2} - x\right) dx,
$$

$$
\int_0^{x_M} \sinh^2 \omega x \, dx = \frac{1}{2} \int_0^{x_M} (\cosh 2\omega x - 1) \, dx = \frac{1}{4\omega} \sinh 2\omega x_M - \frac{1}{2} x_M
$$

$$
\approx \frac{1}{8\omega} e^{2\omega x_M} - \frac{1}{2} x_M = \frac{1}{8\omega} e^{(1-M)\omega L} - \frac{(1-M)\,\omega L}{4},
$$

$$
\int_{x_M}^{L/2} \sinh^2 \omega \left(\frac{L}{2} - x\right) dx = \frac{1}{2} \int_0^{L/2 - x_M} (\cosh 2\omega x - 1) \, dx
$$

$$= \frac{1}{4\omega} \sinh\left(\omega L - 2\omega x_M\right) - \frac{1}{2}\left(\frac{L}{2} - x_M\right)$$

$$\approx \frac{1}{8\omega} e^{\omega L - 2\omega x_M} - \frac{1}{4}\left(L - 2x_M\right) = \frac{1}{8\omega} e^{M\omega L} - \frac{M\omega L}{4},$$

$$\int_0^{L/2} S_x^2 \, dx \approx \omega^2 S_1^2 \left(e^{-(1-M)\omega L}\left(\frac{1}{8\omega} e^{(1-M)\omega L} - \frac{(1-M)\,\omega L}{4}\right)\right.$$

$$\left. + e^{-M\omega L}\left(\frac{1}{8\omega} e^{M\omega L} - \frac{M\omega L}{4}\right)\right) \approx \frac{\omega}{4} S_1^2.$$

For the second integral in (48) we can take into account that $u(0) \approx 0$, that is

$$\int_0^{L/2} \frac{(u - u(0))^2}{u(1-u)} \, dx \approx \int_0^{L/2} \frac{u}{1-u} \, dx \approx \int_{x_M}^{L/2} \frac{dx}{1-u}$$

here we use $0 < x < x_M$ $u(x) \approx 0$. For $x_M < x < L/2$ approximately $S \approx S_1$,

$$u = \frac{1}{1 + e^{S_0 - S}} \approx \frac{1}{1 + e^{-\eta/(2\beta)}}, \quad \frac{1}{1-u} \approx 1 + e^{\eta/(2\beta)}.$$

Since $e^{\eta/(2\beta)} \gg 1$, we can omit 1, and then

$$\int_{x_M}^{L/2} \frac{dx}{1-u} \approx e^{\eta/(2\beta)}\left(\frac{L}{2} - x_M\right) = \frac{ML}{2} e^{\eta/(2\beta)}.$$

The above analysis leads for L large enough to

$$\nu\left(\frac{\omega}{4} S_1^2 + \frac{\eta M L}{2 D_1} e^{\eta/(2\beta)}\right) = \omega^4 S_1^2 \exp\left(-\omega M L\right).$$

We substitute $S_1 = \eta/\beta$ and get an estimate γ_{1A} for the leading order eigenvalue

$$\gamma_{1A} \approx \frac{4 D_1 \omega^4 S_1^2 \exp\left(-M\omega L\right)}{\omega D_1 S_1^2 + 2\eta M L \exp\left(\eta/(2\beta)\right)} \approx \frac{2 D_1 \eta}{ML} \exp\left(-\omega M L - \frac{\eta}{2\beta}\right).$$

A.2. B-pattern

We consider S as given in (51).

$$S_{xx}(0) \approx \omega^2 A \approx \omega^2 S_1 \exp\left(-(1-M)\omega \frac{L}{2}\right),$$

For the first integral we obtain the same estimate

$$\int_0^{L/2} S_x^2 \, dx \approx \frac{\omega}{4} S_1^2,$$

For the second integral we can take into account that $u(0) \approx 1$, that is

$$\int_0^{L/2} \frac{(u - u(0))^2}{u(1-u)} \, dx \approx \int_0^{L/2} \frac{1-u}{u} \, dx \approx \int_{x_M}^{L/2} \frac{dx}{u},$$

here we take into account that for $0 < x < x_M \ u(x) \approx 1$. For $x_M < x < L/2$ approximately $S \approx S_2 \approx 0$,

$$u = \frac{1}{1 + e^{S_0 - S}} \approx \frac{1}{1 + e^{\eta/(2\beta)}}, \qquad \frac{1}{u} \approx 1 + e^{\eta/(2\beta)} \approx e^{\eta/(2\beta)}$$

then

$$\int_{x_M}^{L/2} \frac{dx}{u} \approx e^{\eta/(2\beta)} \left(\frac{L}{2} - x_M \right) = \frac{(1-M)L}{2} e^{\eta/(2\beta)}.$$

This gives

$$\gamma_{1B} \approx \frac{4 D_1 \omega^4 S_1^2 \exp\left(-(1-M)\omega L \right)}{\omega D_1 S_1^2 + 2\eta (1-M)L \exp\left(\eta/(2\beta) \right)} \approx \frac{2 D_1 \eta}{(1-M)L} \exp\left(-\omega(1-M)L - \frac{\eta}{2\beta} \right).$$

REFERENCES

1. Alikakos, N., Bates, P. W., and Fusco, P. (1991). Slow motion for the Cahn-Hilliard equation in one space dimension. *J. Differential Equations* **90**, 81–135.
2. Crutchfield, J. P., and Kaneko, K. (1998). Are attractors relevant to turbulence? *Phys. Rev. Lett.* **60**, 2715–2718.
3. Dolak, Y., and Hillen, T. (2003). Cattaneo models for chemotaxis, numerical solution and pattern formation. *J. Math. Biol.* **46**(2), 153–170.
4. Dolak, Y., and Schmeiser, C. (2004). The Keller-Segel model with small diffusion. *ANUM-Preprint*, 10/04, 1–22.
5. Grinfeld, M., and Novick-Cohen, A. (1999). The viscous Cahn–Hilliard equation: Morse decomposition and structure of the global attractor. *Trans. Am. Math. Soc.* **351**(6), 2375–2406.
6. Hillen, T., and Painter, K. (2001). Global existence for a parabolic chemotaxis model with prevention of overcrowding. *Adv. Appl. Math.* **26**(4), 280–301.
7. Horstmann, D. (2003). From 1970 until present: The Keller-Segel model in chemotaxis and its consequences I. *Jahresbericht der DMV* **105**(3), 103–165.
8. Horstmann, D. (2004). From 1970 until present: The Keller-Segel model in chemotaxis and its consequences II. *Jahresbericht der DMV* **106**(2), 51–69.
9. Iron, D., and Ward, J. (2004). The stability and dynamics of hot-spot solutions for two one-dimensional microwave heating models. *Anal. Appl.* **2**(1), 21–77.
10. Keller, E. F., and Segel, L. A. (1971). Model for chemotaxis. *J. Theor. Biol.* **30**, 225–234.
11. Murray, J. D. (1989). *Mathematical Biology*, Springer, Berlin.
12. Painter, K., and Hillen, T. (2002). Volume-filling and quorum-sensing in models for chemosensitive movement. *Can. Appl. Math. Q.* **10**(4), 501–543.
13. Patlak, C. S. (1953). Random walk with persistence and external bias. *Bull. Math. Biophys.* **15**, 311–338.

14. Schaaf, R. (1985). Stationary solutions of chemotaxis systems. *Trans. AMS* **292**(2), 531–556.

15. Sleeman B. D., Ward M. J., and Wei J. C. (2005). The Existence and Stability of Spike Patterns in a Chemotaxis Model. SIAM *J. Appl. Math.* **65**(3), 790–817.

16. Sun, X., and Ward, M. (2000). Dynamics and coarsening of interfaces for the viscous Cahn-Hilliard equation in one spatial dimension. *Stud. Appl. Math.* **105**, 203–234.